Modelling turbulent collision of bidisperse inertial particles

By YONG ZHOU, ANTHONY S. WEXLER
AND LIAN-PING WANG†

Department of Mechanical Engineering, 126 Spencer Laboratory, University of Delaware, Newark, DE 19716, USA

We study finite-inertia effects on the collision rate of bidisperse heavy particles in a turbulent gas, using direct numerical simulations and kinematic descriptions. As shown previously for a monodisperse system (Sundaram & Collins 1997; Wang, Wexler & Zhou 2000), a statistical mechanical description of the average collision kernel consists of two parts, namely a description of the relative velocity between two colliding particles (the turbulent transport effect) and of the non-uniform particle distribution due to dynamic interaction of particles with coherent vortex structures (the accumulation effect). We first show that this description remains valid and accurate for a bidisperse system involving two groups of particles of inertial response time τ_{p1} and τ_{p2}, respectively. Numerical results for the turbulent transport effect and the accumulation effect have been obtained as a function of τ_{p1} and τ_{p2}. Interestingly, the accumulation effect in a bidisperse system is bounded above by that of a monodisperse system. An explanation for this observation is given, in terms of the correlation between concentration fields of the two size groups. Simulations show that particles from two size groups were found in different regions of a vortex, thus reducing the net accumulation effect in a bidisperse system. The turbulent transport effect, on the other hand, is bounded below by the level in a monodisperse system, due to a differential inertia effect. The above observations imply that the size polydispersity enhances the turbulent transport effect but weakens the accumulation effect, relative to a monodisperse system.

A simple eddy–particle interaction (EPI) model was developed and shown to give a reasonable prediction of the collision kernel, except for a small parametric region where both τ_{p1} and τ_{p2} are on the order of the flow Kolmogorov time τ_k and thus the accumulation effect must be included. A more accurate model incorporating both the turbulent transport effect and the accumulation effect has also been developed. The model would provide an upper bound on the collision rates for a non-dilute bidisperse system, since turbulence modulation and particle–particle interactions are not considered in this model.

Finally, some consideration is given to the effect of nonlinear drag on the collision kernel. The results show that the drag nonlinearity can increase the collision kernel slightly (less than 10%) at large particle inertia.

1. Introduction

Turbulent coagulation, the process of collision-induced merging of particles, in a suspension of solid particles or liquid droplets plays an important role in many natural

† Author to whom correspondence should be addressed, e-mail: lwang@me.udel.edu

and industrial processes. Examples include growth of liquid droplets in turbulent clouds (East & Marshall 1954; Saffman & Turner 1956; Pinsky & Khain 1997; Shaw *et al.* 1998) or in wet steam generators (Williams & Crane 1979), spray atomization process (O'Rourke & Bracco 1980), dust separation in cyclones (Abrahamson 1975), and TiO_2 production (Xiong & Pratsinis 1991). In these applications, the particle density is much larger than that of the carrier fluid and there exists a wide range of particle sizes. When the level of turbulence, as measured by the average rate of kinetic energy dissipation $\bar{\epsilon}$, is large and thus the time scale for small-scale turbulence (the Kolmogorov time scale τ_k) is small, the particle inertial effects, as measured by the ratio of particle response time τ_p to the Kolmogorov time of the turbulent carrier flow τ_k, tend to be important. Therefore, inertial effects resulting from dynamic interactions of particles with turbulent fluid motion at finite τ_p/τ_k must be considered as important factors in the turbulent coagulation process.

The overall coagulation rate of finite-size particles in fluid turbulence is governed by three consecutive and inter-related processes: (i) geometric collision due to turbulent advection, gravitational settling, and Brownian diffusion; (ii) collision efficiency due to local particle–particle aerodynamic interactions; and (iii) coagulation efficiency as determined by surface sticking characteristics (such as van der Waals force, particle wetness, and electrostatic charges). Here we consider only the geometric collision, for which two inertia-induced mechanisms have been identified: (i) the relative velocities between two colliding particles due to turbulent fluctuations of the carrier fluid (Saffman & Turner 1956; Williams & Crane 1983); (ii) the tendency of inertial particles to concentrate within certain regions of turbulent flow (e.g. Maxey 1987; Squires & Eaton 1991; Wang & Maxey 1993). We shall term the first mechanism the turbulent transport effect and the second the accumulation effect. It has been demonstrated that both these inertia-induced effects can lead to one to two orders of magnitude increase in the average collision kernel (Sundaram & Collins 1997; Zhou, Wexler & Wang 1998; Wang, Wexler & Zhou 2000) and a much faster broadening of the droplet size spectrum than previously believed (Pinsky & Khain 1997; Shaw *et al.* 1998).

In our recent paper (Wang *et al.* 2000), we confirmed the statistical mechanical description proposed by Sundaram & Collins (1997) and Wang *et al.* (1998*b*), for a monodisperse system of finite-inertia particles. In Wang *et al.* (2000), we also developed quantitative models for the turbulent transport effect and the accumulation effect, based on direct simulation results of the collision process. We also showed that both these effects increase with flow Reynolds number for finite-inertia particles. A detailed review of the geometric collision literature and the two physical effects is given in Wang *et al.* (2000).

In this study we extend the results of Wang *et al.* (2000) to a bidisperse system of finite-inertia particles. We consider the geometric collision rate between one group of particles of inertial response time τ_{p1} and another group of particles of inertial response time τ_{p2}. In a turbulent flow with velocity fluctuations of a wide range of time scales, the two particle groups may selectively respond to eddies of completely different scales. This differential inertia effect does not occur in a monodisperse system but must be carefully considered in order to model collision rates between any two different particle size groups. We shall show that certain relationships between a bidisperse system and a monodisperse system can be used to construct an approximate model of the bidisperse collision rates.

In the next section we present theoretical considerations relevant to the collision kernel in a bidisperse system. We extend an eddy–particle interaction (EPI) model

(Zhou *et al.* 1998) to a bidisperse system. A brief description of the numerical methods is given in §3. The results of numerical simulations are shown in §4, where we validate the formulation of average collision kernel as given in §2 and compare the EPI model with numerical results. In §5 we develop empirical models to predict the turbulent transport effect, the accumulation effect, and the collision kernel in a bidisperse system. The effect of the flow Taylor-microscale Reynolds number on the collision kernel is discussed in §6, along with the effect of nonlinear drag. Finally, main conclusions are drawn in §7.

2. Theory

We consider a bidisperse suspension of rigid particles in a turbulent gas. The particles are assumed to be small, with diameters d_{p1} and d_{p2} typically on the order of or less than the Kolmogorov length scale $\eta \equiv (v^3/\bar{\epsilon})^{1/4}$, where $\bar{\epsilon}$ is the average rate of dissipation of kinetic energy and v the fluid kinematic viscosity. The particle density ρ_p is much larger than the fluid density ρ so that the particle inertial response time

$$\tau_{pi} = \frac{\rho_p}{\rho} \frac{d_{pi}^2}{18v} \quad \text{for} \quad i = 1, 2, \tag{2.1}$$

may have a magnitude anywhere from the flow Kolmogorov time $\tau_k \equiv (v/\bar{\epsilon})^{1/2}$ to the flow integral time scale T_e.

As a first step towards the modelling of particle collision statistics, we assume that particle volume fraction and mass loading are sufficiently low so that the gas turbulence is not significantly affected by the presence of particles. This assumption may be questionable even in dilute flows due to preferential concentration. Local particle accumulation can introduce local hydrodynamic interactions which are likely to reduce the level of accumulation; therefore, the collision rate obtained in this paper should be viewed as an upper bound for the system considered. Another simplification is that the gravitational (or body force) effect is not included. This assumption is made to allow us to focus on the effect of particle inertia and interphase drag, as in other related studies (Abrahamson 1975; Williams & Crane 1983; Sundaram & Collins 1997). Although the description of gravitational collision alone is well established, our understanding of the couplings between the particle inertia and settling on particle–particle collisions remains incomplete (Reuter, Villiers de & Yavin 1988; Pinsky & Khain 1994; Wang & Maxey 1993; Khain & Pinsky 1995).

The geometric collision rate per unit volume, $\dot{\mathcal{N}}_{12}$, between two size groups of average number concentrations n_1 and n_2 can be written as

$$\langle \dot{\mathcal{N}}_{12} \rangle = \langle \Gamma_{12} \rangle n_1 n_2, \tag{2.2}$$

where $\langle \Gamma_{12} \rangle$ is the average collision kernel. Here $\langle \ \rangle$ denotes an ensemble average, which is equivalent to a spatial average, denoted by $\overline{()}$, for a stationary homogeneous system. Specifically, the ensemble average is taken as a combined average over space, time, and initial realizations (called a triple averaging procedure by Wang & Maxey 1993). For notational simplicity, hereafter we will drop $\langle \ \rangle$ but the ensemble average is always implied when Γ_{12} is mentioned.

The geometric collision kernel can depend on particle and flow parameters:

$$\Gamma_{12} = f(R, \tau_{p1}, \tau_{p2}, u', T_e, v, \bar{\epsilon}, \ldots), \tag{2.3}$$

where the arguments are the collision radius $R \equiv (d_{p1} + d_{p2})/2$, particle response time

in each group, turbulent r.m.s. fluctuation velocity u', integral time T_e, fluid viscosity v, and the average dissipation rate $\bar{\epsilon}$, among other things. Here u' and T_e represent the effect of large-scale turbulent transport on the collision kernel, and v and $\bar{\epsilon}$ describe the effect of small-scale fluid motion. If $d_{p1}, d_{p2} \lesssim \eta$, the average collision kernel can be viewed as a local concentration-squared weighted average of the local collision kernel (Zhou *et al.* 1998), and the local collision kernel is related to the relative velocity between two approaching particles and the collision radius (Saffman & Turner 1956). Large-scale turbulent fluctuations affect Γ_{12} mainly through their contribution to the relative velocity, and this effect becomes dominant if the particle inertial response time is comparable to T_e. Small-scale turbulent fluctuations can affect Γ_{12} mainly through their contributions to non-uniform local particle concentration (Wang & Maxey 1993; Sundaram & Collins 1997; Zhou *et al.* 1998). This accumulation effect becomes important when the particle inertia response time is on the order of τ_k.

Rewriting (2.3) in a dimensionless form, the dimensionless collision kernel is a function of at least four non-dimensional parameters:

$$\frac{\Gamma_{12}}{R^3/\tau_k} \approx f\left(\frac{\tau_{p1}}{\tau_k}, \frac{\tau_{p2}}{\tau_k}, \frac{R}{\eta}, R_\lambda\right), \qquad (2.4)$$

where the Taylor-microscale Reynolds number is defined as $R_\lambda \equiv u'\lambda/v$, where λ is the transverse Taylor microscale $\lambda \equiv u'/\langle(\partial u_1/\partial x_1)^2\rangle^{1/2} = (15vu'^2/\bar{\epsilon})^{1/2}$.

When $d_{p1}, d_{p2} < \eta$, the local shear rate around a particle is nearly uniform and equal to the local velocity gradient. Without considering local particle–particle hydro-dynamic interactions, the turbulent transport effect should be insensitive to the size parameter R/η. However, particles may accumulate indefinitely around a vortex structure, leading to small-scale features in the particle concentration fields at scales less than η. This may cause a strong dependence of the radial distribution function (RDF) on the size parameter R/η, as demonstrated by Reade & Collins (2000). It is reasonable to expect that this size dependence would saturate when the local particle–particle hydrodynamic interactions are considered. In this study we simply fix $R/\eta = 1$ and consider the dependence of Γ_{12} on the other three parameters.

2.1. *The collision kernel formulation*

As demonstrated previously for a monodisperse system (see Sundaram & Collins 1997 and Wang *et al.* 1998*b*, 2000 for details), the average collision kernel can be written as

$$\Gamma_{12} = 2\pi R^2 \langle|w_r|\rangle g_{12}(R). \qquad (2.5)$$

Here w_r is the radial relative velocity between a particle from size group 1 and another particle from size group 2. The average radial relative velocity, $\langle|w_r|\rangle$, represents the turbulent transport effect. Also, $g_{ij}(R)$ denotes the RDF at contact between a particle from group i and another particle from size group j; $g_{12}(R)$ measures the net accumulation effect. In §4, we shall demonstrate numerically that this formulation is rather accurate for a bidisperse system, by comparing it with the collision kernel obtained by direct counting of collision events.

In a monodisperse system, $g_{11}(R)$ is defined as the probability density of observing a particle pair at contact in the actual suspension, normalized by the corresponding value in a nominally uniform suspension. Therefore, $g_{11}(R)$ measures directly the level of particle pair accumulation. However, in a bi-disperse system, $g_{12}(R)$ is determined not only by the level of particle accumulation in each group, but also by the correlation

between particle concentrations in the two groups. This issue will be further illustrated in § 5.

2.2. *The collision kernel for large particle inertia: an eddy–particle interaction model*

When both the inertia parameters τ_{p1} and τ_{p2} are on the order of T_e, the particle concentration fields are nearly uniform. In this case, $g_{12}(R)$ is close to one, in other words the accumulation effect is insignificant. The turbulent transport effect is governed by the interactions of particles with large-scale fluid velocity fluctuations. As a qualitative predictive tool, we can extend the EPI model that we developed previously (Zhou *et al.* 1998) to a bidisperse system.

Let $v^{(1)}$ and $v^{(2)}$ be the radial velocities of the two particles at collision. Assuming the relative velocity $w_r \equiv v^{(2)} - v^{(1)}$ between two colliding particles follows a Gaussian distribution with a standard deviation σ_w, then $\langle |w_r| \rangle = (2/\pi)^{1/2} \sigma_w$. The collision kernel can be written as

$$\langle \Gamma_{12} \rangle = 2\pi R^2 \langle |w_r| \rangle = 2(2\pi)^{1/2} R^2 \sigma_w, \tag{2.6}$$

where

$$\begin{aligned}
\sigma_w &= \langle w_r^2 \rangle^{1/2} = [\langle (v^{(2)} - v^{(1)})^2 \rangle]^{1/2} \\
&= [v_{p1}'^2 + v_{p2}'^2 - 2\langle v^{(1)} v^{(2)} \rangle]^{1/2}. \tag{2.7}
\end{aligned}$$

Here v_{p1}' and v_{p2}' are the particle r.m.s. fluctuation velocities.

In the EPI model, we treat the particle motion as a succession of interactions with turbulent eddies, where each eddy has constant flow properties. More specifically, we consider a one-dimensional version of the particle equation of motion

$$\frac{\mathrm{d}v(t)}{\mathrm{d}t} = \frac{u - v}{\tau_{pi}}, \tag{2.8}$$

where the fluid velocity u is treated as a Monte-Carlo process with a fixed eddy lifetime T (Wang & Stock 1992). The fluid velocity is assumed to take a Gaussian random value in each eddy with a standard deviation equal to the r.m.s. fluid fluctuation velocity u'. The particle velocity variance $(v_{pi}')^2$ is related to the fluid velocity correlation $R_f(\tau) \equiv \langle u(t)u(t + \tau) \rangle$ by (Wang & Stock 1993)

$$(v_{pi}')^2 \equiv \langle v^2(t) \rangle = \frac{1}{\tau_{pi}} \int_0^\infty R_f(\tau) \exp\left(-\frac{\tau}{\tau_{pi}}\right) \mathrm{d}\tau. \tag{2.9}$$

For a Monte-Carlo process, R_f is a triangle function (Wang & Stock 1992)

$$R_f(\tau) = \begin{cases} u'^2(1 - \tau/T) & \text{for} \quad |\tau| < T \\ 0 & \text{for} \quad |\tau| \geqslant T. \end{cases} \tag{2.10}$$

Substituting (2.10) into (2.9), we obtain a relationship between the particle and fluid kinetic energies

$$\frac{(v_{p\alpha}')^2}{u'^2} = 1 - \theta_\alpha[1 - \exp(-1/\theta_\alpha)], \tag{2.11}$$

where $\theta_\alpha \equiv \tau_{p\alpha}/T$.

Next we need to estimate the velocity correlation between two colliding particles, $\langle v^{(1)} v^{(2)} \rangle$. If the particle size is very small, the two particles must be found in the same eddy upon collision. We further assume that the two particles enter the eddy at the

same time, say, $t = 0$. Then by integrating (2.8) the particle velocities can be written as

$$v^{(\alpha)}(t) = u_e \left[1 - \exp\left(-\frac{t}{\tau_{p\alpha}}\right) \right] + v^{(\alpha)}(0) \exp\left(-\frac{t}{\tau_{p\alpha}}\right) \quad \text{for} \quad 0 < t < T, \alpha = 1, 2, \quad (2.12)$$

where $v^{(\alpha)}(0)$ denotes the particle velocity at $t = 0$, and u_e is the eddy velocity. Before entering the eddy ($t < 0$), the two particles interact independently with different eddies so that $\langle v^{(1)}(0)v^{(2)}(0)\rangle = \langle v^{(1)}(0)u_e\rangle = \langle v^{(2)}(0)u_e\rangle = 0$. If the probability distribution for the two particles to collide in the time interval $0 < t < T$ is uniform, then the velocity correlation is

$$\langle v^{(1)}v^{(2)}\rangle = \frac{1}{T} \int_0^T \langle v^{(1)}(t)v^{(2)}(t)\rangle \, \mathrm{d}t. \quad (2.13)$$

Substituting (2.12) into (2.13), we obtain

$$\frac{\langle v^{(1)}v^{(2)}\rangle}{u'^2} = 1 - \theta_1 \left[1 - \exp\left(-\frac{1}{\theta_1}\right) \right]$$

$$-\theta_2 \left[1 - \exp\left(-\frac{1}{\theta_2}\right) \right] + \theta_{12} \left[1 - \exp\left(-\frac{1}{\theta_{12}}\right) \right], \quad (2.14)$$

where $\theta_\alpha = \tau_{p\alpha}/T$, $\theta_{12} = \theta_1\theta_2/(\theta_1 + \theta_2)$.

An expression for σ_w can be obtained by substituting (2.11) and (2.14) into (2.7). Finally the collision kernel is

$$\langle \Gamma_{12} \rangle = 2(2\pi)^{1/2} R^2 u' [\Theta_1 + \Theta_2 - 2\Theta_{12}]^{1/2}, \quad (2.15)$$

where $\Theta_\alpha = \theta_\alpha[1 - \exp(-1/\theta_\alpha)]$, $\Theta_{12} = \theta_{12}[1 - \exp(-1/\theta_{12})]$. The eddy lifetime T is simply set to the large-eddy turnover time T_e when the above model is compared with numerical results in §4. The correlation coefficient of the particle velocities is given as

$$\rho_{12}^v \equiv \frac{\langle v^{(1)}v^{(2)}\rangle}{v'_{p1}v'_{p2}} = \frac{1 - \Theta_1 - \Theta_2 + 2\Theta_{12}}{[(1 - \Theta_1)(1 - \Theta_2)]^{1/2}}. \quad (2.16)$$

It should be noted that the above analysis does not include the eddy size effect, which can modify the EPI time as the particles may traverse the eddy in a time less than T. Also, velocity shear within an eddy is not considered. Nevertheless, the model captures the essential physics of relative motion between two particles and, as will be shown in §4, gives reasonable predictions when τ_{pi} is on the order of T_e.

3. Numerical simulations

Direct numerical simulations provide a means to understand the essential physical mechanisms of turbulent collision and a database to examine new and old analytical models (e.g. Sundaram & Collins 1997; Wang *et al.* 1998*a*, 2000; Zhou *et al.* 1998). There are four components to the development of numerical methods for turbulent collision of inertial particles: (*a*) direct numerical simulation of gas turbulent flow, (*b*) particle tracking, (*c*) collision rate detection, and (*d*) computation of relative velocity and radial distribution function. For a monodisperse system, each of these has been described in detail in Wang *et al.* (2000). Therefore we shall only provide essential information about the flow field, and comment on issues pertinent to a bidisperse system.

Grid resolution	64^3	96^3
u'	18.22	18.30
$\bar{\epsilon}$	3421.0	3554.7
v	0.238	0.139
R_λ	45	58
η	0.0450	0.0294
τ_k	0.00830	0.00625
T_e	0.097	0.094
T_e/τ_k	11.7	15.0

TABLE 1. Flow characteristics.

3.1. *Flow field*

A homogeneous and isotropic turbulent flow was generated by full numerical simulations using a pseudo-spectral method. The incompressible Navier–Stokes equations

$$\frac{\partial \boldsymbol{u}}{\partial t} = \boldsymbol{u} \times \boldsymbol{\omega} - \nabla \left(\frac{P}{\rho} + \tfrac{1}{2}\boldsymbol{u}^2 \right) + v\nabla^2 \boldsymbol{u} + \boldsymbol{f}(\boldsymbol{x},t), \tag{3.1}$$

were solved along with the continuity equation $\nabla \cdot \boldsymbol{u} = 0$ in a periodic box of side 2π. Here $\boldsymbol{\omega} \equiv \nabla \times \boldsymbol{u}$ is the vorticity, P is the pressure. The flow was generated from rest by the random forcing term $\boldsymbol{f}(\boldsymbol{x},t)$ which is non-zero only at low wavenumbers, $|\boldsymbol{k}| < 8^{1/2}$.

In this paper, the flow was frozen after the statistically stationary stage was reached, and particles were then introduced into the flow. The start of particle release will be denoted as $t = 0$. This provides us with an identical flow microstructure for different runs with various particle parameters, which limits statistical fluctuations and speeds data collection.

Since all the important flow scales are resolved in a full numerical simulation, the grid resolution determines the scale separation, and thus the Reynolds number of the resulting flow. Two grid resolutions of 64^3 and 96^3 were used to study briefly the effect of Taylor-microscale Reynolds number on the collision kernel (table 1).

Table 1 lists the flow parameters (from top to bottom): the component r.m.s. fluctuating velocity u', average dissipation rate $\bar{\epsilon}$, viscosity v, Taylor-microscale Reynolds number $R_\lambda \equiv u'\lambda/v$, Kolmogorov length η, Kolmogorov time τ_k, large-eddy turnover time $T_e \equiv u'^2/\bar{\epsilon}$, and the time scale ratio T_e/τ_k. Other details of the simulated flows can be found in Wang & Maxey (1993).

3.2. *Particle motion*

Under the assumption that the density of the particle ρ_p is much larger than the density of the fluid ρ, and that a quasi-steady Stokes drag can be used, the equation of motion for a heavy particle becomes

$$\frac{\mathrm{d}\boldsymbol{V}(t)}{\mathrm{d}t} = \frac{\boldsymbol{u}(\boldsymbol{Y}(t),t) - \boldsymbol{V}(t)}{\tau_{pi}}, \tag{3.2}$$

where $\boldsymbol{V}(t)$ and $\boldsymbol{Y}(t)$ are the velocity and the centre position of a heavy particle, respectively.

Typically 10^3–10^4 particles for each size group were introduced at $t = 0$ into the computational domain at random initial positions with an initial velocity equal to the local fluid velocity. After about $3 \times \max(\tau_{p1}, \tau_{p2})$, any effects of the initial conditions

on the particle motion became lost. The simulation was continued for at least $13 \times \max(\tau_{p1}, \tau_{p2})$ or 5 large-eddy turnover times during which collision counts and other statistical averages were taken. It should be noted that the particle concentration field and the local-in-time collision kernels may not reach their asymptotic, statistically stationary stage at $t = 3 \max(\tau_{p1}, \tau_{p2})$ since the local accumulation process is affected by large-scale fluid motion (Wang & Maxey 1993). On the other hand, in practical applications one may be more interested in the particle collision statistics shortly after the particle release rather than the asymptotic value. With this in mind and for the purpose of obtaining a small numerical uncertainty, we take $t = 3 \max(\tau_{p1}, \tau_{p2})$ as the starting time for all statistical averages. A change of the starting time to $t = 2T_e$ showed that the results change less than 20% and are unchanged qualitatively.

3.3. *Collision rate* $\dot{\mathcal{N}}_{12}$

The collision detection algorithm used to compute $\dot{\mathcal{N}}_{12}$ is similar to that of Wang *et al.* (2000) for a monodisperse system. There could be different approaches to perform a numerical simulation of turbulent collisions for a polydisperse system. One of these is that particles are allowed to grow in time. When two particles are in contact with each other, a new larger particle will be formed. The number of collisions between any two different size groups can be counted, then the collision kernel can be directly calculated. This would be the natural way for a coagulative system. However, it is an impractical method to study the parametric dependence of the collision kernel. First, many more particles are needed in such a polydisperse system, since the total number of particles has to be divided by the number of size groups. Second, a stationary particle size distribution is desired to obtain good statistics of the collision kernel, but may be difficult to maintain. We, therefore, choose to separate the microphysical modelling (estimation of collision kernel between any given two size groups) from the macrophysical process (the evolution of particle size distribution). We introduce only two particle size groups of inertial response times τ_{p1} and τ_{p2}. A collision is counted if a new geometric overlap is encountered. Only the collision events between two different size groups are considered. The two particles upon a collision continue to move independently (Scheme 1 in Wang *et al.* 1998a). This post-collision treatment may sound unrealistic; however, it was shown to be the only scheme that is consistent with the Saffman & Turner (1956) formulation. Use of this scheme will facilitate the validation procedure for independent, separate quantifications of the turbulent transport effect and the local accumulation effect (see §3.4). Another advantage of using this scheme is that we can calculate the radial distribution function at contact $g(R)$ accurately.

We only consider binary collisions as the particle loadings are sufficiently dilute in our numerical simulations. The collision search was conducted using the efficient cell-index method and the concept of linked lists (Allen & Tildesley 1987). The size of the collision detection cell was made large enough so that two particles residing in unconnected cells would not collide within a numerical time step (Sundaram & Collins 1996; Wang *et al.* 1998a). Averages over both time and initial realizations of particle locations were used to reduce the numerical uncertainties. The collision kernel based on direct counting of collisions will be denoted by

$$\Gamma_{12}^{DNS} \equiv \frac{\dot{\mathcal{N}}_{12}}{n_1 \, n_2}. \tag{3.3}$$

We had validated our bidisperse simulation code by comparing the result when $\tau_{p1} = \tau_{p2}$ with that of our previous monodisperse code.

3.4. *Relative velocities and $g_{12}(R)$*

The Lagrangian-pair relative velocity statistics ($\langle |w_r| \rangle$) measures the turbulent transport effect, while the radial distribution function at contact $g_{12}(R)$ quantifies the accumulation effect. Their computations were completely independent of the collision kernel simulation. The computational procedure is as follows.

(*a*) Particle pair identification: at each time step, we detected all the pairs (with one particle from each size group) with interparticle distance r given as $R - \delta/2 < r < R + \delta/2$ with $\delta = 2\%$ R. This detection was performed using the same efficient cell-index method and the concept of linked lists. However, the size of the detection grid, W, could now be made much smaller than was needed for the collision kernel simulation. In fact, $W = R + \delta/2$ is sufficient for the detection. Obviously only a fraction of these pairs will participate in collision events during the next numerical time step. The value of δ/R should be selected properly (see Wang *et al.* 2000).

(*b*) $g_{12}(R)$ and $\langle |w_r| \rangle$ calculation: the simulation was run for the same period of time as in the collision kernel computation and the initial $3 \max(\tau_{p1}, \tau_{p2})$ time interval was not used for statistical averaging. All the pairs of separation $R - \delta/2 < r < R + \delta/2$, along with individual particle velocities and the separation vectors, were recorded during the simulation. These data were postprocessed to give an average value for $|w_r|$ and $g_{12}(R)$ for that run. For example, $g(R)$ was computed simply as

$$g_{12}(R) = \frac{\text{Total number of pairs detected} \times V_{box}}{V_s \times N_t \times N_{p1} N_{p2}}, \tag{3.4}$$

where N_{p1} and N_{p2} are total number of particles in the two size groups, $V_s = 4\pi[(R + \delta/2)^3 - (R - \delta/2)^3]/3$ is the shell volume, $V_{box} = (2\pi)^3$ is the volume of the flow domain, and N_t is the number of time steps for which the pair detections were undertaken.

(*c*) Improving the statistics: the simulation was repeated N_r times with independent realizations of the initial particle locations, as in the collision kernel simulation. This then allows a further averaging over the realizations (thus further reducing the uncertainties) and, more importantly, an estimation of statistical uncertainties can be made. Note that the records in a given realization may not be independent when dt is small. But the averaged values over time from different realizations can be treated as independent samples.

The computation of $g_{12}(R)$ and $\langle |w_r| \rangle$ was validated against the monodisperse results (Wang *et al.* 2000). For the purpose of presenting results in subsequent discussions, we denote the collision kernels estimated with numerical kinematic properties of the suspension as

$$\Gamma_{12}^{est} = 2\pi R^2 \langle |w_r| \rangle g_{12}(R). \tag{3.5}$$

In summary, the collision kernel measures dynamical events which are related to the change of inter-particle distance, while both relative velocities and $g_{12}(R)$ are kinematic quantities which are defined at any given time. In numerical simulations, since the time step size is finite, the dynamic and kinematic properties must be computed separately.

4. Results and discussion

4.1. *Numerical results for arbitrary inertia*

Figure 1 shows the numerical collision kernels Γ_{12}^{DNS}, normalized by the collision kernel for fluid elements (zero-inertia particles) $\Gamma_0 = (8\pi/15)^{1/2} R^3 v_k/\eta$ (Saffman &
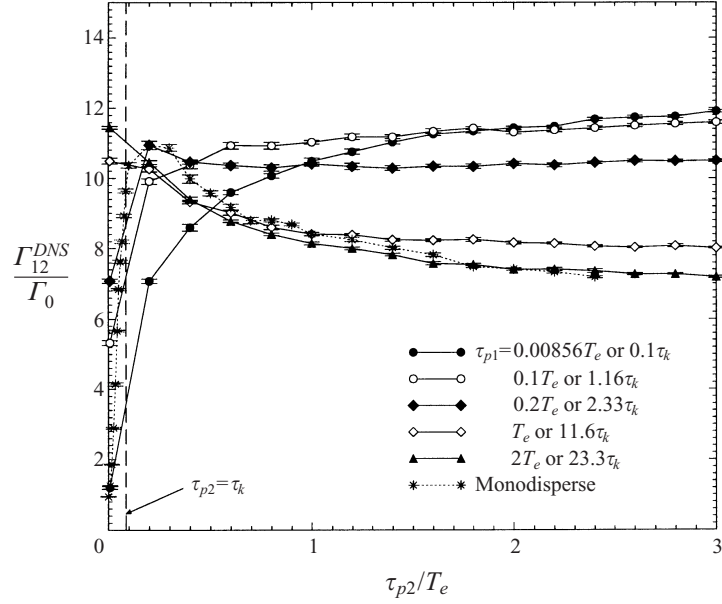
FIGURE 1. Numerical collision kernels, normalized by Γ_0, as a function of τ_{p2}/T_e at $R_\lambda = 45$, while τ_{p1}/T_e was fixed for each curve. The error bars denote $\pm\sigma$ (the standard deviation).
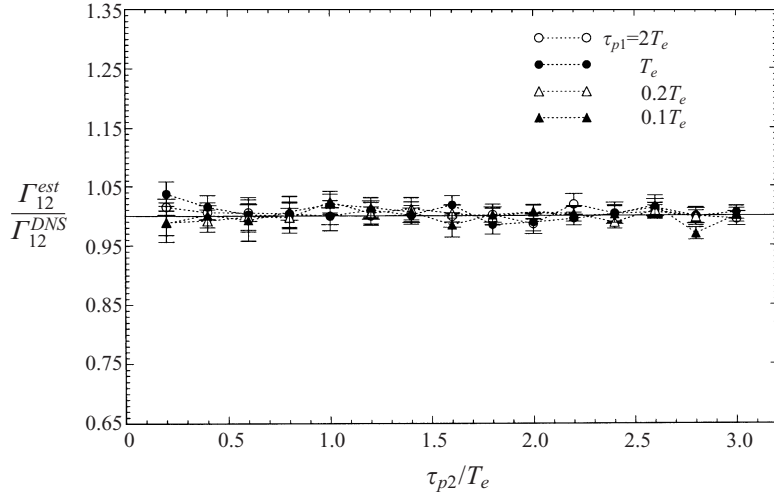

FIGURE 2. Comparison of Γ_{12}^{est} with Γ_{12}^{DNS}.

Turner 1956), as a function of τ_{p2}/T_e at $R_\lambda = 45$, while τ_{p1}/T_e was fixed for each curve. The error bars denote twice the standard deviation, which were estimated based on 12 runs with independent realizations of particle initial locations. Also shown in this figure is the collision kernel for a monodisperse system. For small τ_{p1}/τ_k, Γ_{12}^{DNS} increases with τ_{p2} monotonically, mainly due to the increasing relative motion of particles in the second size group from the fluid. For large τ_{p1}/T_e, Γ_{12}^{DNS} decreases with τ_{p2} monotonically, due to the increasingly sluggish response of particles in the second size group to the turbulent fluid velocity fluctuations. Note that for both these limits of τ_{p1} the accumulation effect is not important. For intermediate τ_{p1},
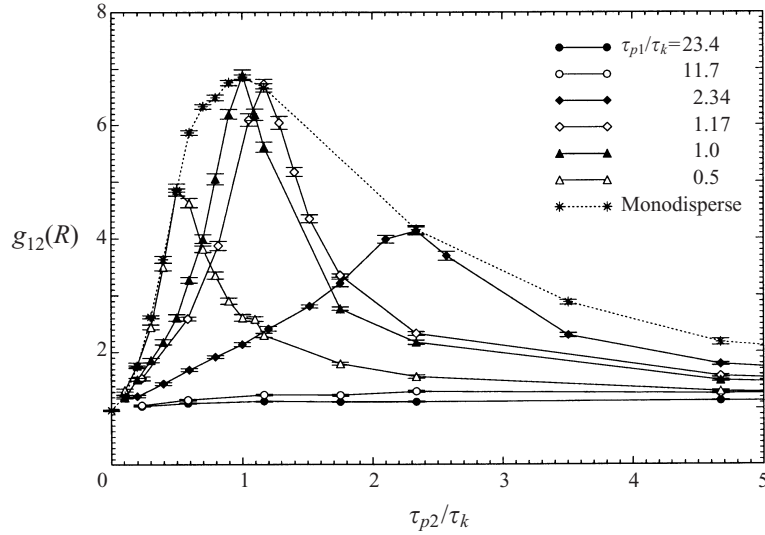
FIGURE 3. The bidisperse RDF, $g_{12}(R)$, as a function of τ_{p2}/τ_k.

Γ_{12}^{DNS} can increase with τ_{p2} for small τ_{p2}, reach a maximum, and then decrease with τ_{p2}. This complex dependence reflects the interplay of small- and large-scale fluid motions and the selective response of particles to these dynamics. If the accumulation effect is negligible ($\tau_{p1}, \tau_{p2} \ll \tau_k$ or $\tau_{p1}, \tau_{p2} \gg \tau_k$), the bidisperse collision kernel is larger than the monodisperse value due to the differential in the inertia effect on the relative velocity between the two size groups. When the accumulation effect is strong ($\tau_{p1}/\tau_k, \tau_{p2}/\tau_k = O(1)$), the bidisperse collision kernel is less than the monodisperse value due to lack of correlation between the particle concentration fields of the two size groups (see § 5.1).

In figure 2 we confirm the statistical formulation, (2.5), by plotting the ratio $\Gamma_{12}^{est}/\Gamma_{12}^{DNS}$ for different combinations of particle inertias. The ratio should be one if the formulation (2.5) is exact. This is confirmed within numerical uncertainties. Therefore, (2.5) can be used to predict the collision kernel in a bidisperse system, extending the conclusion established previously for the monodisperse case (Wang *et al.* 2000).

4.2. *Separation of the accumulation effect and the turbulent transport effect*

Confirmation of the formulation (2.5) allows us to separate the accumulation effect from the turbulent transport effect. Figure 3 shows the radial distribution function at contact $g_{12}(R)$, namely the accumulation effect on the collision kernel. The curve marked monodisperse denotes the value of $g_{22}(R)$ or RDF at contact for a monodisperse system with particle response time τ_{p2} (e.g. see Wang *et al.* 2000). Two interesting observations can be made: (i) $g_{12}(R)$ attains a maximum when $\tau_{p2} = \tau_{p1}$, and (ii) $g_{12}(R)$ is always bounded above by the smaller value of the two relevant monodisperse RDFs, namely $g_{12}(R) \leqslant \min[g_{11}(R), g_{22}(R)]$. An explanation for these observations will be given in § 5.1.

The turbulent transport effect on the collision kernel is measured in figure 4. The radial relative velocity $\langle |w_r| \rangle$, normalized by the fluid r.m.s. velocity u', is shown as a function of τ_{p2}/T_e, for different τ_{p1}. For convenience, we introduce the following notation: $\langle |w_r| \rangle_{12} \equiv \langle |w_r| \rangle(\tau_{p1}, \tau_{p2})$, $\langle |w_r| \rangle_{11} \equiv \langle |w_r| \rangle(\tau_{p1}, \tau_{p1})$, $\langle |w_r| \rangle_{22} \equiv \langle |w_r| \rangle(\tau_{p2}, \tau_{p2})$. The
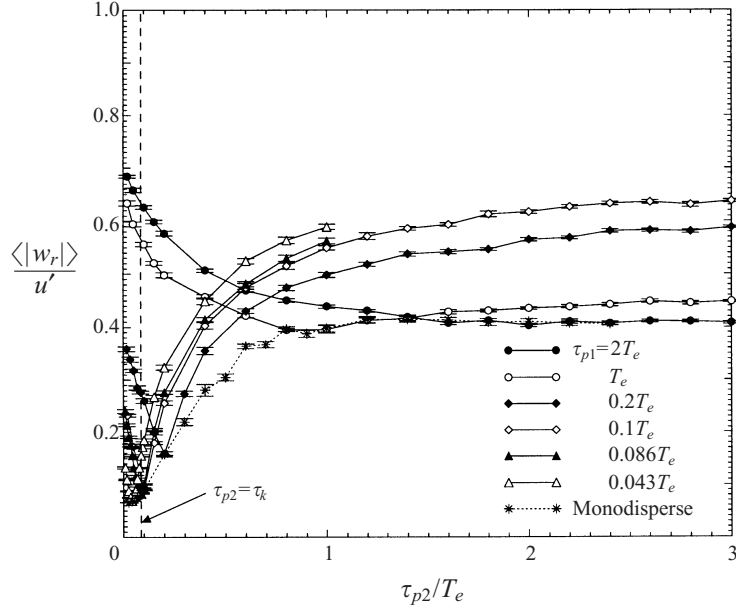
FIGURE 4. The radial relative velocity $\langle|w_r|\rangle$, normalized by the fluid r.m.s. velocity u', as a function of particle inertia τ_{p2}/T_e.
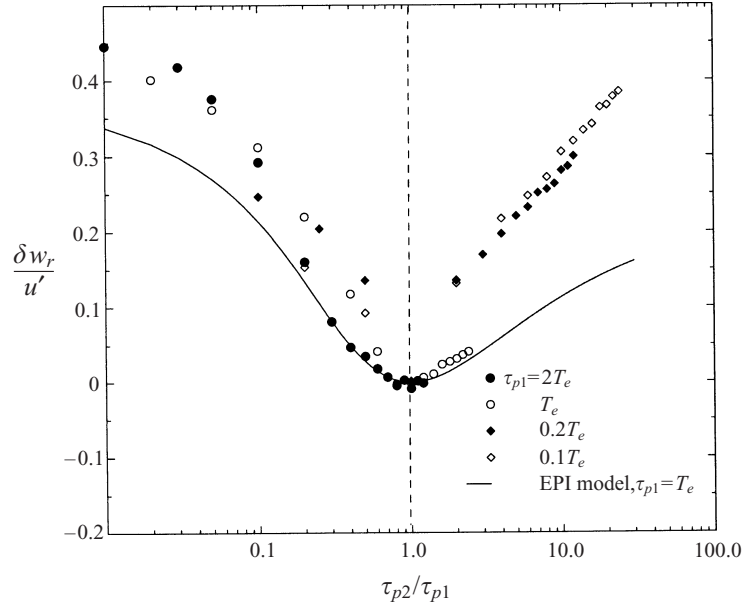

FIGURE 5. δw_r as a function of τ_{p2}/τ_{p1}.

curve labelled as monodisperse in figure 4 denotes the value of $\langle|w_r|\rangle_{22}$. By comparing with the monodisperse data (dotted line), we find that the difference in particle inertias enhances the radial relative velocity (the differential inertia effect), namely $\langle|w_r|\rangle_{12} \geqslant \max[\langle|w_r|\rangle_{12} \geqslant \max[\langle|w_r|\rangle_{11}, \langle|w_r|\rangle_{22}]$. Therefore, $\langle|w_r|\rangle$ in a bidisperse system is always larger than that in a monodisperse system. This is in qualitative agreement with the analytical results of Kruis & Kusters (1997).
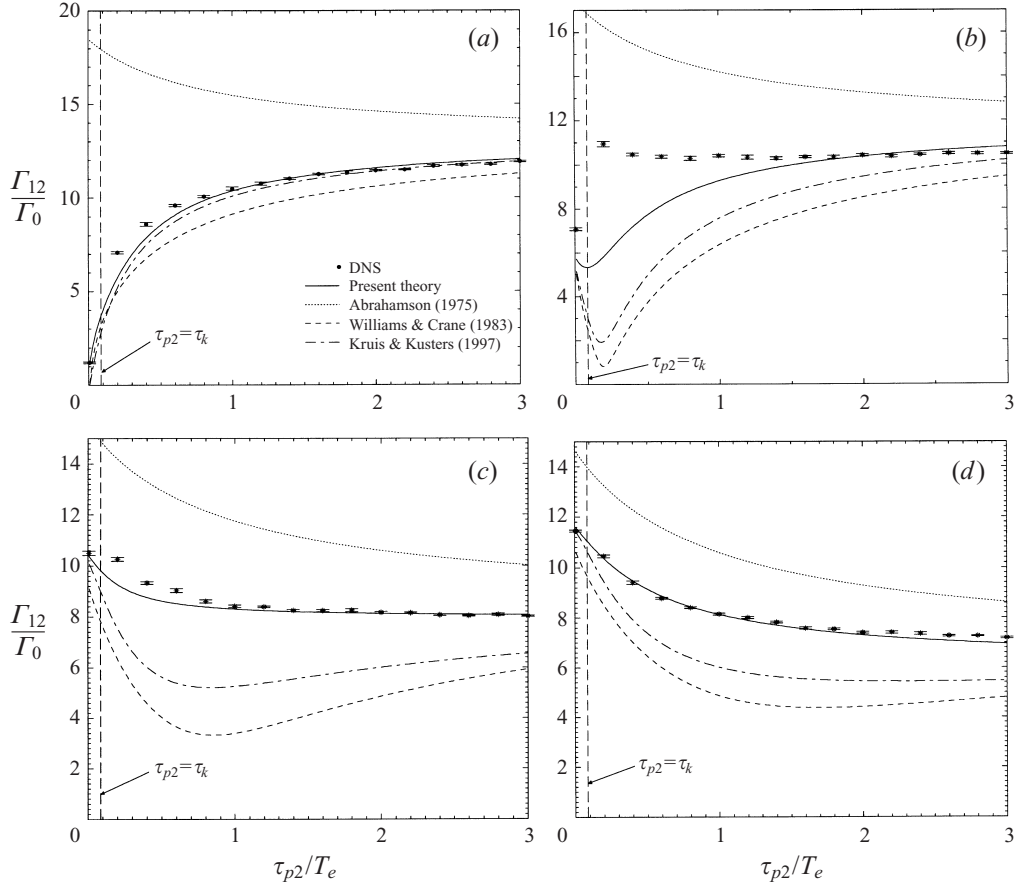
FIGURE 6. Comparison of the theoretical results with numerical simulations: The error bars denote $\pm\sigma$ (the standard deviation). $R_\lambda = 45$. (a) $\tau_{p1}/T_e = 0.0086$ or $\tau_{p1}/\tau_k = 0.1$; (b) $\tau_{p1}/T_e = 0.2$ or $\tau_{p1}/\tau_k = 2.3$; (c) $\tau_{p1}/T_e = 1.0$ or $\tau_{p1}/\tau_k = 11.7$; (d) $\tau_{p1}/T_e = 2.0$ or $\tau_{p1}/\tau_k = 23.4$.

The larger the inertia difference between the two size groups, the more the radial relative velocity increases above the monodisperse value. This is demonstrated in figure 5 which shows the additional increase in the relative velocity above the average of the two relevant monodisperse values, $\delta w_r \equiv \langle |w_r| \rangle_{12} - \frac{1}{2}(\langle |w_r| \rangle_{11} + \langle |w_r| \rangle_{22})$. This additional increase δw_r due to the inertia difference is precisely what we mean by the differential inertia effect. Note that δw_r is symmetric with respect to (τ_{p1}, τ_{p2}), i.e. the two response times are interchangeable. Under the assumption that this additional increase is mainly a function of τ_{p2}/τ_{p1} (the leading-order reduction of two independent variables to one), a symmetry would be observed with respect to $\log_{10}(\tau_{p2}/\tau_{p1})$. This symmetry is shown to be roughly valid in figure 5, although the above leading-order reduction has no rigorous justification. Also shown in figure 5 is the prediction of the EPI model for $\tau_{p1} = T_e$.

4.3. *Comparison of the EPI model with simulation results*

Before developing a more accurate model, we shall compare the EPI model and other existing collision kernel models with simulation results. All these models do not include the accumulation effect here.

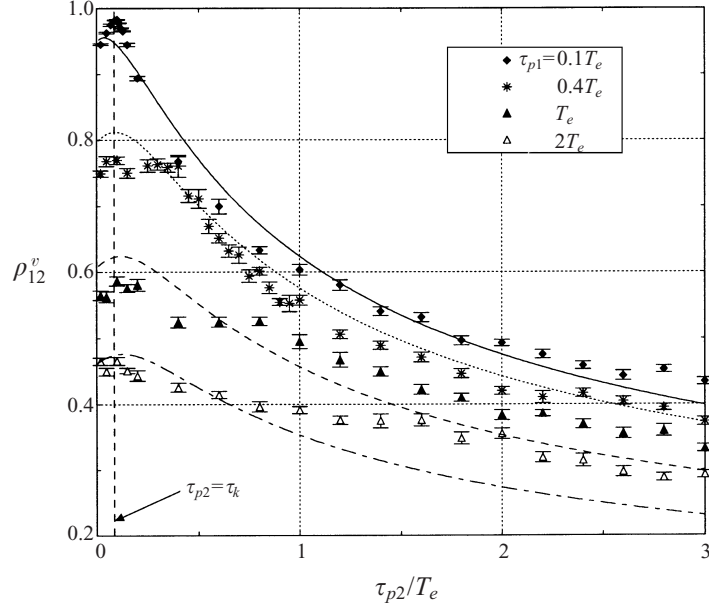Figure 6 shows such comparisons at $R_\lambda = 45$. Each of figures 6(*a*)–6(*d*) assumes

FIGURE 7. The particle velocity correlation coefficient ρ_{12}^v as a function of τ_{p2}/T_e. The symbols represent DNS results. The lines represent predictions of the EPI model, (2.16).

a fixed τ_{p1}/T_e, at 0.0086, 0.2, 1.0, and 2.0 respectively. Besides the EPI model, the theoretical predictions of Abrahamson (1975), Williams & Crane (1983), and Kruis & Kusters (1997) are also plotted.

For small τ_{p1}/τ_k (figure 6a), particles in the first size group are nearly uniformly distributed. Both the EPI model, (2.15), and the model of Kruis & Kusters (1997) predict a collision kernel to within 15% of simulation results.

When τ_{p1}/τ_k is on the order of unity (figure 6b), particles in the first size group are highly non-uniformly distributed. It is not surprising to see that none of the models predicts well for $\tau_{p2}/T_e < 1.0$, due to the accumulation effect not being considered in these models. Nevertheless, the models appear to work well for $\tau_{p2}/T_e > 1.0$, with a relative difference of less than 10%.

When τ_{p1} is on the order of the integral time scale T_e (figures 6c and 6d), the accumulation effect can again be neglected. Interestingly our simple EPI model gives the best prediction (to within 10% of the simulation results).

The general observation is that the EPI model performs well if either τ_{p1} or τ_{p2} is on the order of the integral time scale T_e. In all the cases, the formulation of Kruis & Kusters (1997) provides a better prediction of the collision kernel than the Williams & Crane (1983) formulation, but they both tend to underpredict the collision kernel. The model of Abrahamson (1975) overpredicts the collision kernel due to the assumption of zero correlation between velocities of colliding particles.

Figure 7 shows the velocity correlation coefficient ρ_{12}^v as a function of τ_{p2}/T_e. The symbols represent the DNS data, and the lines represent the predictions by the EPI model, (2.16). For most parametric regions, ρ_{12}^v decreases as τ_{p1} or τ_{p2} increases, as a result of increasing departure of the particle motion from the local fluid flow. The model agrees with DNS results to within 15% of relative difference when $\rho_{12}^v > 0.4$, and shows that ρ_{12}^v drops slowly for large τ_{p2}/T_e.

5. Model development

We shall now develop a model to predict the turbulent transport effect and the accumulation effect for a bidisperse system, based on the model we developed previously for a monodisperse system (Wang *et al.* 2000) and the numerical results presented here for a bidisperse system.

5.1. *The relationship between RDFs in bidisperse and monodisperse systems*

First we shall postulate a relationship between the RDF $g_{12}(R)$ of a bidisperse system and the RDFs $g_{11}(R)$ and $g_{22}(R)$ of a monodisperse system in order to simplify the modelling of $g_{12}(R)$.

We start by hypothesizing that the probability of finding a pair (τ_{p1}, τ_{p2}) with a separation $R \pm \delta$ locally is proportional to $c_1 c_2$, where c_1 and c_2 are the local number densities for the two size groups. This is a reasonable hypothesis if the particles in both size groups are randomly distributed within any local volume over which the concentrations are defined. Therefore the average RDFs can be related to the local particle number concentrations as

$$g_{12}(R) \approx \frac{\overline{c_1 c_2}}{\overline{c_1}\,\overline{c_2}}, \quad g_{11}(R) \approx \frac{\overline{c_1^2}}{(\overline{c_1})^2}, \quad g_{22}(R) \approx \frac{\overline{c_2^2}}{(\overline{c_2})^2}, \tag{5.1}$$

where the overline denotes spatial or ensemble averaging.

Consider a total of N_p particles randomly distributed in a volume V. Assume that this volume is divided uniformly into N_c cells and that the local number concentration in each cell is simply defined as the number of particles realized in that cell divided by the cell volume (V/N_c). The probability of finding k particles (or local number density kN_c/V) in any cell is

$$p(c = kN_c/V) = \binom{N_p}{k} p^k (1-p)^{n-k} \tag{5.2}$$

with $p = 1/N_c$. It follows that

$$\overline{c} = \frac{N_p}{V} \quad \text{and} \quad \overline{c^2} = (\overline{c})^2 + \frac{N_p(N_c - 1)}{V^2}. \tag{5.3}$$

Therefore, for a random spatial distribution of particles, we have

$$\frac{\overline{c^2}}{(\overline{c})^2} = 1 + \frac{N_c - 1}{N_p}. \tag{5.4}$$

This would be consistent with the fact that $g_{11}(R)$ approaches one if $N_p \gg N_c$.

For an actual turbulent suspension, both $g_{11}(R)$ and $g_{22}(R)$ may be larger than one if there is some degree of preferential concentration for the two size groups. Defining the correlation coefficient between two concentration fields as

$$\rho_{12}^n = \frac{\overline{(c_1 - \overline{c_1})(c_2 - \overline{c_2})}}{[\overline{(c_1 - \overline{c_1})^2}\,\overline{(c_2 - \overline{c_2})^2}]^{1/2}}, \tag{5.5}$$

we can show that

$$g_{12}(R) = 1 + \rho_{12}^n [(g_{11}(R) - 1)(g_{22}(R) - 1)]^{1/2}. \tag{5.6}$$

Intuitively, the correlation coefficient is in the range
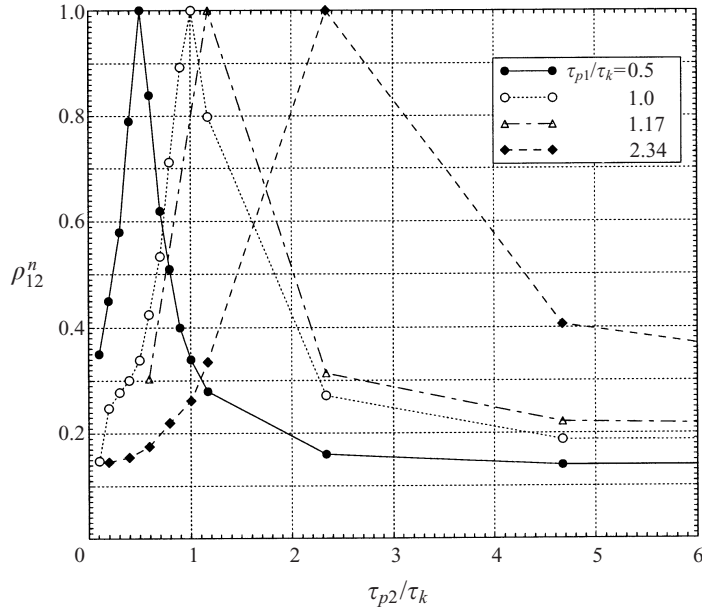
$$0 \leqslant \rho_{12}^n \leqslant 1, \tag{5.7}$$

FIGURE 8. The concentration correlation coefficient ρ_{12}^n as a function of τ_{p2}/τ_k.

since preferential concentration always drives particles into regions of low fluid vorticity and high rate of strain. Equations (5.6) and (5.7) imply that

$$g_{12}(R) \leqslant \max\left[g_{11}(R), g_{22}(R)\right], \qquad (5.8)$$

or the RDF of a bidisperse system is bounded above by the values of the monodisperse system. This inequality is less stringent than the observation in figure 3 that $g_{12}(R) \leqslant \min\left[g_{11}(R), g_{22}(R)\right]$, due to a rapid decrease of the inter-correlation coefficient ρ_{12}^n as τ_{p1} and τ_{p2} depart from each other (see below). Equation (5.6) also provides a useful way to interpret and model the results of $g_{12}(R)$.

5.2. *The concentration correlation coefficient*

An estimate of concentration correlation coefficient ρ_{12}^n can be made using (5.6), the results of $g_{12}(R)$, and the monodisperse RDF (Wang *et al.* 2000). The direct computation of ρ_{12}^n may be useful but requires simulations with many more particles so that the local particle concentration field can be accurately defined. A further study will address this issue. In figure 8 we show the estimated ρ_{12}^n as a function of τ_{p2}/τ_k. We focus on particle inertia response time on the order of τ_k, as this is the parametric region where the accumulation effect is important. The concentration correlation coefficient reaches the maximum value of one at $\tau_{p1} = \tau_{p2}$, and then drops quickly as τ_{p2} departs from τ_{p1}. This suggests that particles with different inertias will be found in different regions relative to the flow microstructures. This is confirmed by a snapshot of the particle positions shown in figure 9, in which we plot the locations of a second group of particles in a local region along with the locations of the first group of particles at time $t = 2T_e$ after release. The black and grey circles represent particles with the same response time ($\tau_p = \tau_k$) but independent initial locations. The open circles represent particles with $\tau_p = 0.5\tau_k$ but the same initial locations as grey circles. All the particles are initially randomly distributed. It is evident that particles of the same inertial response time tend to overlap in space even though they
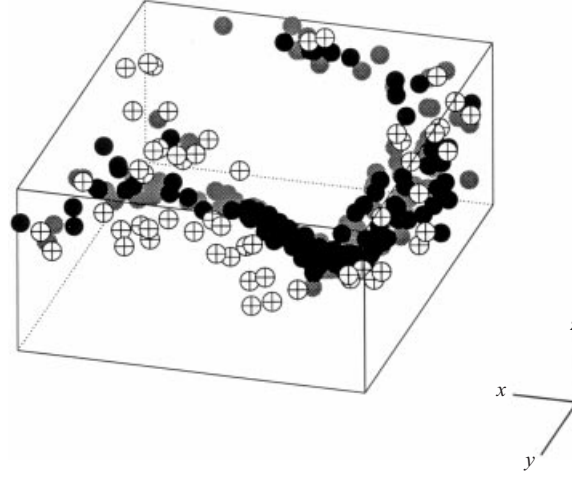
FIGURE 9. A snapshot of particle locations in a local flow region. The box covers a region $22\eta \times 28\eta \times 11\eta$.
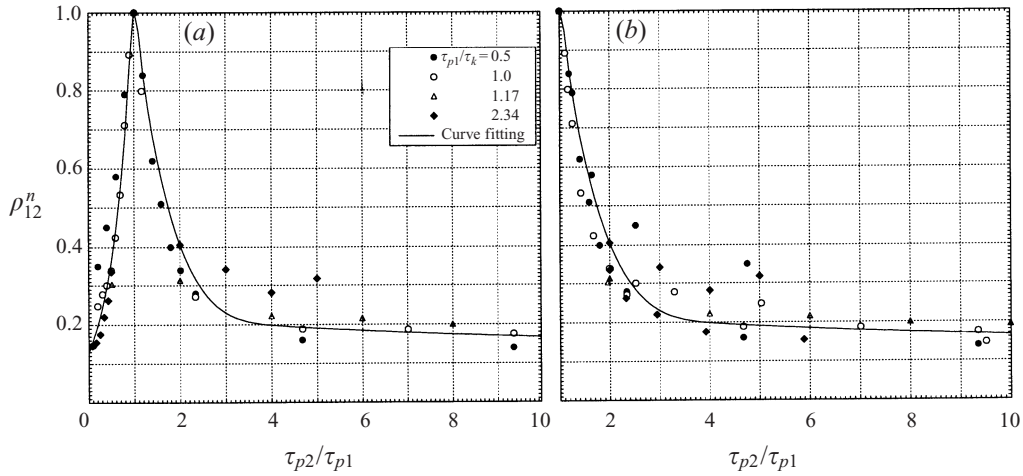

FIGURE 10. The concentration correlation coefficient ρ_{12}^n as a function of τ_{p2}/τ_{p1}. The symbols represent DNS results. The solid line represents the curve fitting, (5.11).

are introduced at different locations initially. The second group of particles with a different τ_p, although accumulating in similar regions as the black and grey particles, do not overlap with them exactly, leading to a low correlation coefficient.

Now the task of modelling $g_{12}(R)$ reduces to the modelling of ρ_{12}^n. To leading order, ρ_{12}^n may be considered a function of τ_{p2}/τ_{p1} only, as shown in figure 10(*a*). Furthermore, since

$$\rho_{12}^n(\tau_{p1}, \tau_{p2}) = \rho_{12}^n(\tau_{p2}, \tau_{p1}),$$

it follows that

$$\rho_{12}^n(\tau_{p2}/\tau_{p1}) \approx \rho_{12}^n(\tau_{p1}/\tau_{p2}).$$

The data for $\tau_{p2}/\tau_{p1} < 1$ in figure 10(*a*) are replotted in figure 10(*b*) at the time scale
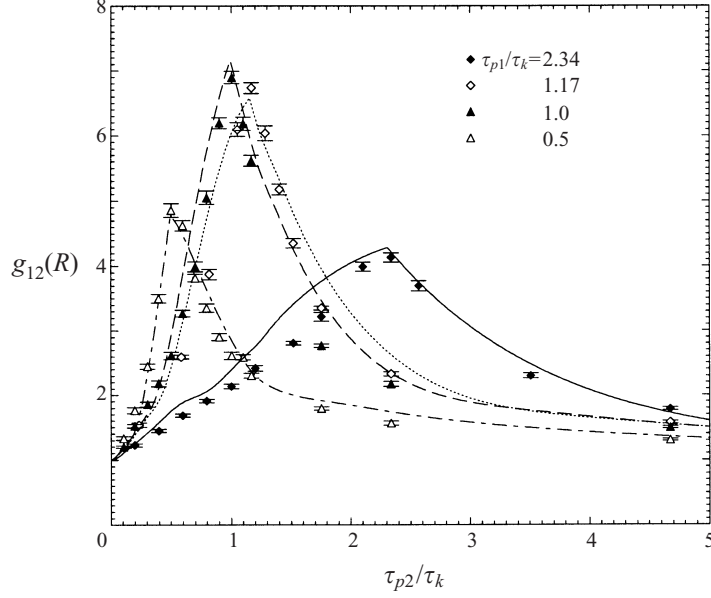
FIGURE 11. Comparison of modelled $g_{12}(R)$ with DNS data. The symbols represent DNS results. The lines represent model predictions using (5.6).

ratio equal to τ_{p1}/τ_{p2} according to the above approximation. The peak locations are now fixed at $\tau_{p2}/\tau_{p1} = 1$. The off-peak data points show some degree of collapse.

As a first approximation, we fit a single curve to the average value of the data in figure 10(*b*). The curve fitting was done by first considering two sub-regions: $1 \leqslant \phi < 2.5$, and $\phi > 2.5$, where $\phi \equiv \tau_{p2}/\tau_{p1}$. These two regions are fitted separately by

$$y_1(\phi) = 2.6 \exp(-\phi) \quad \text{for} \quad 1 < \phi < 2.5, \tag{5.9}$$

$$y_2(\phi) = 0.205 \exp(-0.0206\phi) \quad \text{for} \quad \phi > 2.5. \tag{5.10}$$

A composite fit is then constructed in the following manner:

$$\rho_{12}^n = y_1(\phi) + y_2(\phi)z(\phi), \tag{5.11}$$

where $z(\phi)$ is a smooth transition function defined as

$$z(\phi) = \tfrac{1}{2}[1 + \tanh(\phi - 3)].$$

The composite fit is compared with the simulation data in figure 10(*b*). Using the above fitting for ρ_{12}^n and the model for $g_{11}(R)$ and $g_{22}(R)$ according to Wang *et al.* (2000), the bidisperse RDF can be estimated through (5.6). The resulting model is compared with the simulation data in figure 11. The model agrees with the DNS results to within 10%.

5.3. *The relative velocity*

For the turbulent transport effect we modified the formulation of Kruis & Kusters (1997), as we did for the monodisperse case (Wang *et al.* 2000). Kruis & Kusters (1997) obtained a universal solution for the relative velocity of two particles due to turbulent accelerations by modifying the derivations of Williams & Crane (1983) and
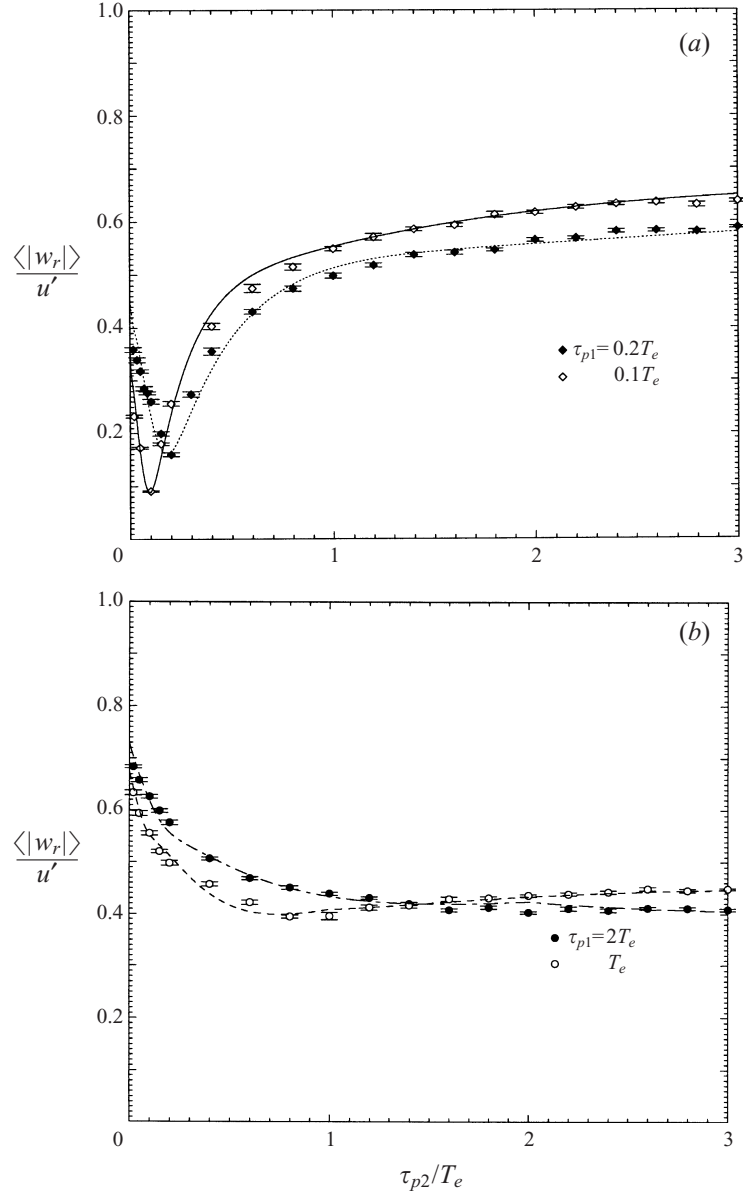
FIGURE 12. Comparison of modelled $\langle |w_r| \rangle$ with DNS data. The symbols represent DNS results. The lines represent model predictions using (5.13).

Yuu (1984). For heavy particles ($\rho_p/\rho_f \gg 1$), their relationship becomes

$$\frac{w^2_{accel,i}}{u'^2} = \frac{\gamma}{\gamma - 1} \left\{ (\theta_1 + \theta_2) - \frac{4\theta_1\theta_2}{(\theta_1 + \theta_2)} \left[\frac{1 + \theta_1 + \theta_2}{(1 + \theta_1)(1 + \theta_2)} \right]^{1/2} \right\}$$

$$\times \left[\frac{1}{(1 + \theta_1)(1 + \theta_2)} - \frac{1}{(1 + \gamma\theta_1)(1 + \gamma\theta_2)} \right], \tag{5.12}$$
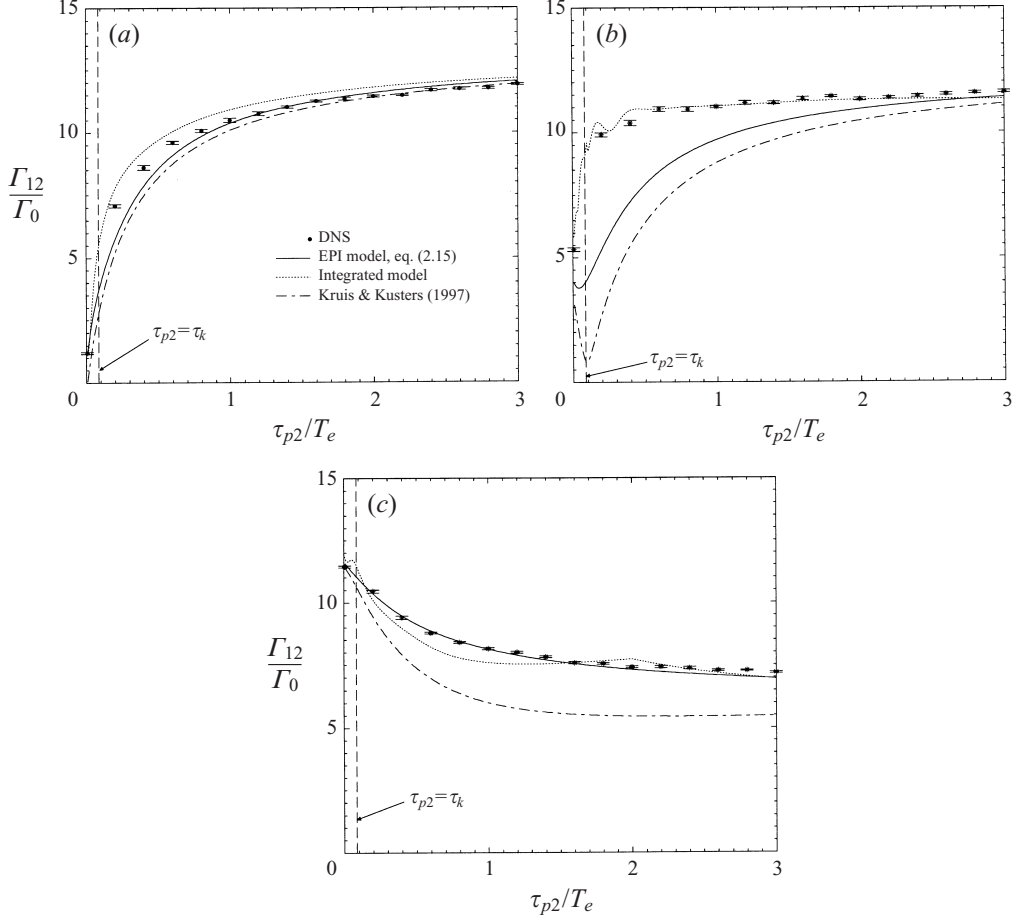
FIGURE 13. Comparison of modelled Γ_{12}/Γ_0 with DNS data. (a) $\tau_{p1} = 0.0086T_e$ or $0.1\tau_k$;
(b) $\tau_{p1} = 0.1T_e$ or $1.17\tau_k$; (c) $\tau_{p1} = 2T_e$ or $23\tau_k$.

where $\theta_\alpha = 2.5\tau_{p\alpha}/T_e$ and $\gamma = 0.183u'^2/(\epsilon v)^{1/2}$. Note that the definition of θ_α here is different from what we used in (2.15).

We modify this equation to fit our numerical results for the radial relative velocity in a similar way to what we did for monodisperse particles (Wang *et al.* 2000) and propose that

$$w^2_{r,accel} = C_w(\alpha)w^2_{accel,i}, \tag{5.13}$$

where

$$C_w(\alpha) = 1.0 + 0.6\exp\left[-(\alpha - 1)^{1.5}\right];$$

here $\alpha = \max\left[\theta_2/\theta_1, \theta_1/\theta_2\right]$. There are two differences between bidisperse and monodisperse formulations for $w_{r,accel}$: first $C_w(\alpha)$ is a function of α in a bidisperse system, but a constant in a monodisperse system; and second γ in (5.13) is also a function of α:

$$\gamma = \alpha \times 0.183\frac{u'^2}{(\epsilon v)^{1/2}}.$$

These modifications have no theoretical justification but result from a trial and error fit to our data. After including the shear effect as in Wang *et al.* (2000), we
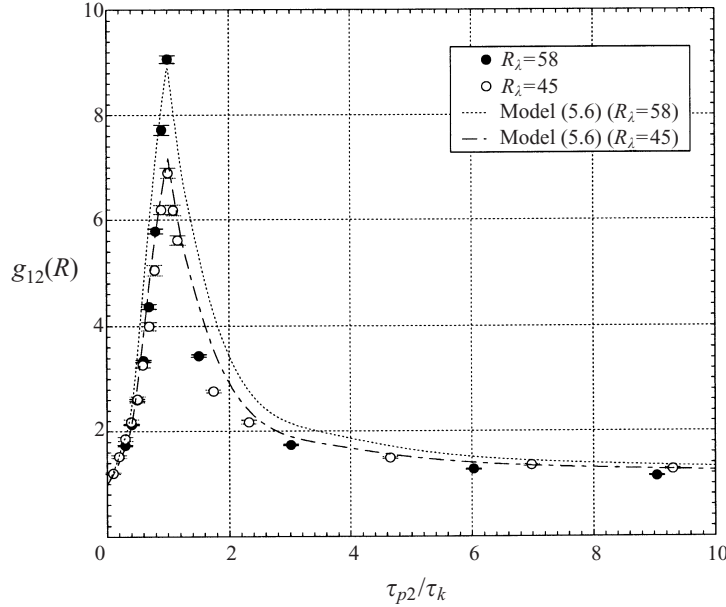
FIGURE 14. Demonstration of the dependence of $g_{12}(R)$ on R_λ. $\tau_{p1}/\tau_k = 1$.

obtain

$$\langle |w_r| \rangle = \left[\frac{2}{\pi} (\langle w_{r,accel}^2 \rangle + \langle w_{r,shear}^2 \rangle) \right]^{1/2}, \quad \text{with} \quad \frac{\langle w_{r,shear}^2 \rangle}{v_k^2} = \frac{1}{15} \left(\frac{R}{\eta} \right)^2; \qquad (5.14)$$

the result is compared with simulation data in figures 12(a) and 12(b). The model shows good agreement with numerical results for almost all combinations of τ_{p1} and τ_{p2}, with a relative difference within 5%.

5.4. *The collision kernel*

Finally, a combination of the above models leads to a model for the collision kernel Γ_{12}, according to (2.5). A comparison of the integrated model with the DNS collision kernel is shown in figure 13(a–c). The model predicts the collision kernel well. The maximum relative error between the model and DNS data is 10%. This level of model accuracy is satisfactory for engineering applications. Also shown in these figures are theoretical predictions of the EPI model and Kruis & Kusters's (1997) formulation. It is clearly seen in figure 13(b) that the integrated model shows a major improvement over other models when both τ_{p1} and τ_{p2} are on the order of τ_k, while the EPI model predicts the collision kernel about 2.5 times lower than DNS data, and the Kruis & Kusters (1997) formulation 10 times lower.

   Although we focus on particle inertia response time comparable to τ_k during the model development for RDF, the final model of Γ_{12} may be used for arbitrary particle inertia since the accumulation effect is not important for either very small or large particle inertia. Figure 13(a) shows the comparison of the estimated Γ_{12} by different models with DNS results for τ_{p1} much less than τ_k, and figure 13(c) shows the comparison for τ_{p1} on the order of T_e. An alternative is simply making use of the EPI model for large particle inertias.
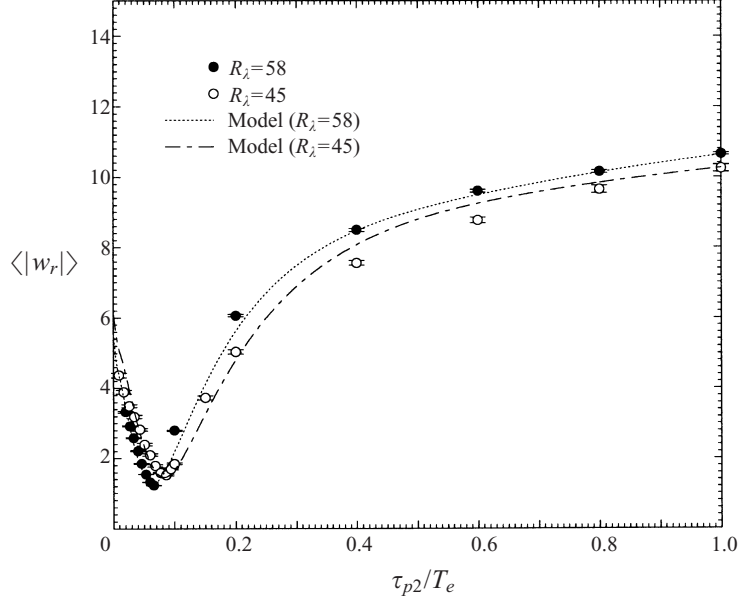
FIGURE 15. Comparison of modelled $\langle |w_r| \rangle$ with DNS data for two different Reynolds numbers. $\tau_{p1}/\tau_k = 1$.

6. Other considerations

6.1. *The effect of flow Reynolds number on the collision kernel*

So far we have discussed results at $R_\lambda = 45$ only. However, the model we developed in the last section is capable of including the flow Reynolds number effect. We have shown that $g(R) - 1$ scales with the Reynolds number R_λ linearly in a monodisperse system (Wang *et al.* 2000), except for $\tau_p/\tau_k < 0.5$. We shall assume that, other than the Reynolds number dependence of $g_{11}(R)$ and $g_{22}(R)$ discussed in Wang *et al.* (2000), the same ρ_{12}^n model can be used for other flow Reynolds numbers. It follows from (5.6) that $g_{12}(R)$ would have a similar Reynolds number scaling as $g_{11}(R)$ and $g_{22}(R)$ if both τ_{p1}/τ_k and τ_{p2}/τ_k are larger than 0.5. This appears to be confirmed in figure 14, although the range of R_λ is rather narrow here.

The model for the turbulent transport effect is compared with the simulation results at two different R_λ in figure 15. The model seems to predict well the modifying effect due to the flow Reynolds number on the radial relative velocity, with less than 5% relative difference from the simulation results.

Finally, the integrated model for the collision kernel is compared with the simulation results at two Reynolds numbers in figure 16. The model can predict the DNS data to within 20%.

6.2. *Effect of nonlinear drag*

In the preceding discussion the fluid drag force on the particle has been based on a linear, Stokes drag law. More generally, a nonlinear relation for the drag force, depending on the particle Reynolds number, should be used if the Reynolds number is not small. In the section a brief discussion is given of the modifying effects of such a nonlinear drag force relation on the average collision kernel.
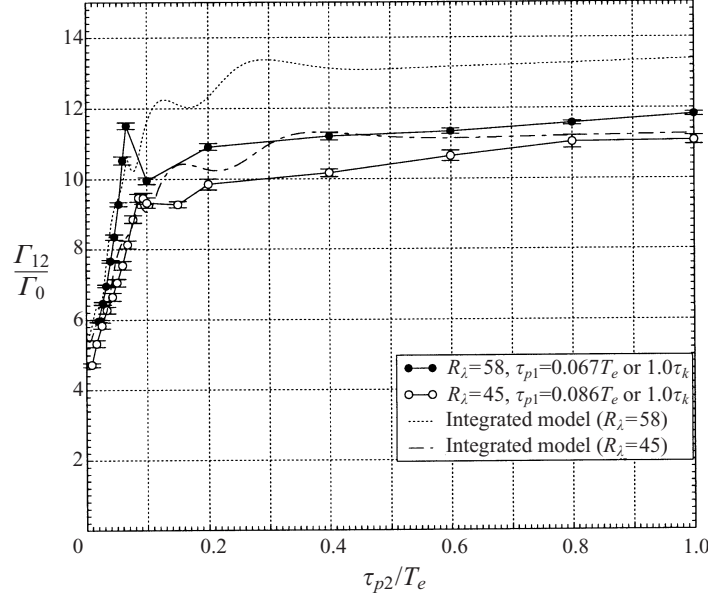
FIGURE 16. Comparison of modelled Γ_{12}/Γ_0 with DNS data for two different Reynolds numbers. The line without symbols represents model predictions. $\tau_{p1}/\tau_k = 1$.

We shall adopt an empirical relationship for the drag coefficient C_D given by Shiller & Naumann (1933):

$$C_D(Re_p) = \frac{24}{Re_p}[1 + 0.15Re_p^{0.687}] = f\frac{24}{Re_p}. \tag{6.1}$$

Then the equation of particle motion becomes

$$\frac{\mathrm{d}V(t)}{\mathrm{d}t} = \frac{f}{\tau_{pi}}[u(Y(t),t) - V(t)], \quad \text{with} \quad f = 1 + 0.15Re_p^{0.687}. \tag{6.2}$$

Here τ_{pi} is the Stokes response time defined in (2.1), the particle Reynolds number is $Re_p \equiv d_{pi}|u - V|/v$.

A set of simulations has been undertaken with $\tau_{p1}/T_e = 1.0$ while τ_{p2}/T_e varied from 0 to 3.0 at $R_\lambda = 45$. The results are shown in figure 17. The nonlinear drag increases the collision kernel slightly (about 10%) for $\tau_{p2}/T_e > 0.2$, which is contrary to speculation by Kruis & Kusters (1997) that the assumption of Stokes' law yields an overestimation of the relative particle velocity w. Our explanation of the results is as follows: since the r.m.s. velocity of large-inertia particles is much smaller than that of the fluid, the nonlinear drag, which is larger than the Stokes drag, will increase the particle r.m.s. velocity rather than decrease it; it follows that relative particle velocity is increased since at large inertia the square of the relative velocity is proportional to the sum of the squares of the two particle fluctuating velocities.

We may further demonstrate this by modifying the EPI model. By taking into account the nonlinear drag, (2.8) becomes

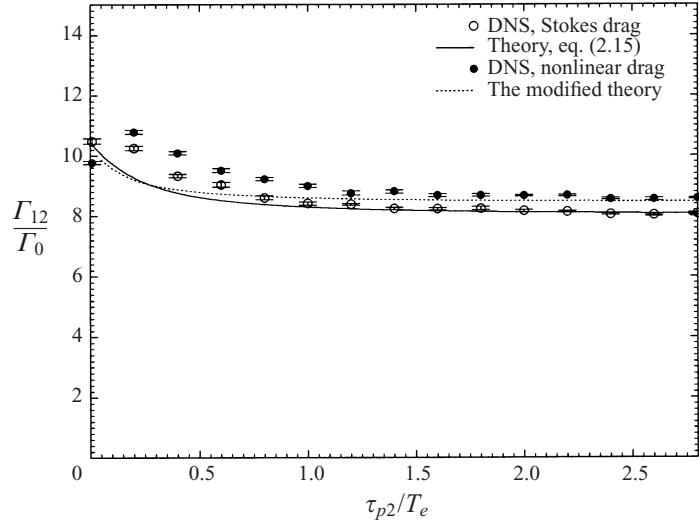$$\frac{\mathrm{d}v(t)}{\mathrm{d}t} = \frac{f}{\tau_{pi}}(u - v). \tag{6.3}$$

FIGURE 17. The effect of nonlinear drag on the collision kernel. $R_\lambda = 45$, $\tau_{p1}/T_e = 1.0$.

This equation can be integrated exactly (Michaelides 1997) to yield the following expression:

$$v^{(\alpha)}(t) = u_e \left\{ 1 - \exp\left(-\frac{t}{\tau_{p\alpha}}\right) \left[1 + 0.15 Re_f^{0.687} \left(1 - \exp\left(-0.687\frac{t}{\tau_{p\alpha}}\right)\right)\right]^{-1.5} \right\}$$

$$+ v^{(\alpha)}(0) \exp\left(-\frac{t}{\tau_{p\alpha}}\right) \left[1 + 0.15 Re_f^{0.687} \left(1 - \exp\left(-0.687\frac{t}{\tau_{p\alpha}}\right)\right)\right]^{-1.5}, \quad (6.4)$$

for $0 < t < T$, $\alpha = 1, 2$, where Re_f is a Reynolds number based on the uniform fluid velocity ($Re_f = d_p u_e / v$). Following the same procedures as in §2.2, we may obtain the particle velocity correlation by substituting (6.4) into (2.13). Since we cannot integrate (2.13) analytically, a numerical integration was used instead. The results based on this modified theory are also shown in figure 17 as a dotted line. It agrees with the DNS results very well for large particle inertia. This again shows that nonlinear drag causes a slight increase in the collision kernel for the parametric range we studied here.

7. Summary

The main objective of this work was to develop a model to predict the geometric collision kernel in a bidisperse system, including both the turbulent transport effect and the accumulation effect. Such a model has been developed based on a previous one for a monodisperse system (Wang *et al.* 2000) and numerical experiments designed to gather data for a bidisperse system. A complete set of numerical experiments requires much more effort because of the number of parameters involved. We focused in this work on various combinations of the particle inertia response times. A brief discussion of flow Reynolds number and nonlinear drag effects was given. The particle size effect has been left out because, unlike other effects, it depends on the local particle–particle interaction model, including local hydrodynamic interactions

and post-collision treatment. A discussion of the size effect in the absence of local hydrodynamic interactions can be found in the work of Reade & Collins (2000).

The numerical simulations undertaken in this study show that the statistical formulation, (2.5), first suggested by Sundaram & Collins (1997) and later improved by Wang *et al.* (1998*b*, 2000) is accurate for a bidisperse system. The simulations help us develop a model for the bidisperse accumulation effect. It was shown that the bidisperse RDF, g_{12}, can be expressed in terms of monodisperse RDFs and a correlation coefficient ρ_{12}^n between the particle concentration fields. Such an expression leads to the conclusion that the bidisperse RDF is bounded above by the values of monodisperse RDFs, which is consistent with the numerical results. Curve fitting ρ_{12}^n as a function of τ_{p2}/τ_{p1} completes the modelling of g_{12}. Physically, g_{12} measures the net accumulation effect as a result of both particle accumulation and spatial correlation between two concentration fields. An interesting observation is that ρ_{12}^n changes very quickly with inertial response times τ_{pi} when τ_{pi} is on the order of the flow Kolmogorov time τ_k. This implies that particles with different inertias will be found in different regions relative to flow microstructures. This is shown by visualization of particle positions in direct numerical simulations. In general, the accumulation effect is less important for a bidisperse system than in a monodisperse system. This implies that there is a much higher possibility of particles with similar inertial response time to collide with each other than those with unlike inertial response times, especially when the particle inertia is on the order of τ_k.

The turbulent transport effect, measured by the radial relative velocity $\langle|w_r|\rangle$, can be modelled by modifying the Kruis & Kusters (1997) formulation. The results show that the turbulent transport effect is enhanced by the difference in particle inertia. $\langle|w_r|\rangle$ in a bidisperse system is bounded below by that in a monodisperse system.

An integrated working model for the collision kernel has been made available for the first time. The model is shown to be satisfactory for engineering applications. We believe that such a model is much needed in future modelling of particle size distribution via population balance equations. For this purpose, we summarize the model as the following. For bidisperse inertial particles under the assumptions $d_{pi} \leqslant \eta$ and $\rho_p \ll \rho$, the collision kernel can be calculated as

$$\frac{\Gamma_{12}}{\Gamma_0} = \frac{\langle|w_r|\rangle_{12}}{\langle|w_r|\rangle_{shear}} g_{12}(R),$$

where $R = r_1 + r_2$, $\Gamma_0 = (8\pi/15)^{1/2} R^3 v_k/\eta$, $\langle|w_r|\rangle_{shear} = (2/15\pi)^{1/2} v_k(R/\eta)$. The average radial relative velocity $\langle|w_r|\rangle$ is computed by

$$\frac{\langle|w_r|\rangle_{12}}{\langle|w_r|\rangle_{shear}} = \left[1 + 15 \frac{w_{r,accel}^2}{v_k^2}\left(\frac{\eta}{R}\right)^2\right]^{1/2},$$

with

$$\frac{w_{r,accel}^2}{v_k^2} = C_w(\phi)\left(\frac{u'}{v_k}\right)^2\frac{\gamma}{\gamma-1}\left\{(\theta_1+\theta_2) - \frac{4\theta_1\theta_2}{(\theta_1+\theta_2)}\left[\frac{1+\theta_1+\theta_2}{(1+\theta_1)(1+\theta_2)}\right]^{1/2}\right\}$$
$$\times\left[\frac{1}{(1+\theta_1)(1+\theta_2)} - \frac{1}{(1+\gamma\theta_1)(1+\gamma\theta_2)}\right],$$

where $\theta_i = 2.5\tau_{pi}/T_e$ and

$$C_w(\phi) = 1.0 + 0.6\exp\left[-(\phi - 1)^{1.5}\right],$$

$$\gamma = \phi \times 0.183\frac{u'^2}{(\epsilon v)^{1/2}},$$

with $\phi \equiv \max(\theta_2/\theta_1, \theta_1/\theta_2)$.

The bidisperse radial distribution function at contact $g_{12}(R)$ is given by

$$g_{12}(R) = 1 + \rho_{12}^n[g_{11}(R) - 1]^{1/2}[g_{22}(R) - 1]^{1/2},$$

with

$$\rho_{12}^n = 2.6\exp(-\psi) + 0.205\exp(-0.0206\psi)\tfrac{1}{2}[1 + \tanh(\psi - 3)],$$

where $\psi \equiv \max(\tau_{p2}/\tau_{p1}, \tau_{p1}/\tau_{p2})$. The monodisperse radial distribution function at contact $g_{ii}(R)$ (no summation is implied) is modelled as

$$g_{ii}(R) = 1 + y_0(\alpha)[1 - z_0^2(\alpha)] + R_\lambda z_0^2(\alpha)\{y_1(\alpha)[1 - z_1(\alpha)] + y_2(\alpha)z_1(\alpha) + y_3(\alpha)z_2(\alpha)\},$$

with

$$y_0(\alpha) = 18\alpha^2, \quad y_1(\alpha) = 0.36\alpha^{2.5}\exp(-\alpha^{2.5}),$$

$$y_2(\alpha) = 0.24\exp(-0.5\alpha), \quad y_3(\alpha) = 0.013\exp(-0.07\alpha),$$

$$z_0(\alpha) = \frac{1}{2}\left[1 + \tanh\frac{\alpha - 0.5}{0.25}\right], \quad z_1(\alpha) = \frac{1}{2}\left[1 + \tanh\frac{\alpha - 1.25}{0.1}\right],$$

$$z_2(\alpha) = \frac{1}{2}\left[1 + \tanh\frac{\alpha - 6.5}{2.5}\right],$$

where $\alpha \equiv \tau_{pi}/\tau_k$. Note that the intermediate symbols used here may be different from those appearing in previous sections to avoid confusion.

The above model can be applied directly, for example, to powder production and cloud droplet growth involving small heavy particles in a turbulent gas. The model would provide an upper bound on the collision rates for a non-dilute bidisperse system, since turbulence modulation and particle–particle interactions are not considered in this model. When the particle density is comparable to the fluid, such as in a slurry, modifications to the above model are needed to include other forces on particles (e.g. Kruis & Kusters 1997). If the particle size is larger than the flow Kolmogorov scale, for example in fluidized bed reactors, other finite-size effects will have to be considered (e.g. **?**).

It should be noted that the model is based on the assumption of isotropic, homogeneous turbulence, which is an idealized condition that is rarely achieved in practice. The different flow structures such as in wall-bounded turbulence or shear flows may require separate treatment. Nevertheless the model may still be a reasonable one for anisotropic flows as long as the flow Reynolds number is large and there is a reasonable separation between the energy-dominated scales and the vorticity-dominated scales of motion. The modelling of the turbulent transport effect in isotropic flows can be done by the eddy–particle interaction model using multiple fluid velocity and length scales.

We have also extended the EPI model (Zhou *et al.* 1998) to a bidisperse system. It has been shown that it can be an accurate alternative when the particle inertia response time is large or very small compared to τ_k. The EPI model can be easily modified to include the nonlinear drag effect.

REFERENCES

ABRAHAMSON, J. 1975 Collision rates of small particles in a vigorously turbulent fluid. *Chem. Engng Sci.* **30**, 1371–1379.

ALLEN, M. P. & TILDESLEY, D. J. 1987 *Computer Simulation of Liquids.* Oxford University Press.

DELICHATSIOS, M. A. 1980 Particle coagulation in steady turbulent flows: application to smoke aging. *J. Colloid Interface Sci.* **78**, 163–174.

EAST, T. W. R. & MARSHALL, J. S. 1954 Turbulence in clouds as a factor in precipitation. *Q. J. R. Met. Soc.* **80**, 26.

FLAGAN, R. C. & SEINFELD, J. H. 1988 *Fundamentals of Air Pollution Engineering.* Prentice Hall.

KHAIN, A. P. & PINSKY, M. B. 1995 Drop inertia and its contribution to turbulent coalescence in convective clouds. Part I. Drop fall in the fall with random horizontal velocity. *J. Atmos. Sci.* **52**, 196–206.

KRUIS, F. E. & KUSTERS, K. A. 1997 The collision rate of particles in turbulent flow. *Chem. Engng Commun.* **158**, 201–230.

MAXEY, M. R. 1987 The gravitational settling of aerosol particles in homogeneous turbulence and random flow fields. *J. Fluid Mech.* **174**, 441–465.

MICHAELIDES, E. E. 1997 Review – The transient equation of motion for particles, bubbles, and droplets. *Trans. ASME*: *J. Fluids Engng* **119**, 233–247.

O'ROURKE, P. J. & BRACCO, F. V. 1980 Modelling of drop interactions in thick sprays and a comparison with experiments. In *Stratified Charge Automotive Engines Conference,* p. 101. The Institution of Mechanical Engineers, London.

PINSKY, M. B. & KHAIN, A. P. 1994 Initiation of drop velocity oscillations during their fall in a vertically sheared flow with embedded velocity fluctuation. *Geophys. Astrophys. Fluid Dyn.* **78**, 169–192.

PINSKY, M. B. & KHAIN, A. P. 1997 Turbulence effects on droplet growth and size distribution in clouds – a review. *J. Aerosol Sci.* **28**, 1177–1214.

READE, W. C. & COLLINS, L. R. 2000 Effect of preferential concentration on turbulent collision rates. *Phys. Fluids* **12**, 2530–2540.

REUTER, G. W., VILLIERS, R. DE & YAVIN, Y. 1988 The collection kernel for two falling cloud drops subjected to random perturbations at a turbulent airflow: A stochastic model. *J. Atmos. Sci.* **45**, 765–773.

SAFFMAN, P. G. & TURNER, J. S. 1956 On the collision of drops in turbulent clouds. *J. Fluid Mech.* **1**, 16–30; also Corrigendum **196**, 1988, 599.

SHAW, R. A., READE, W. C., COLLINS, L. R. & VERLINDE, J. 1998 Preferential concentration of cloud droplets by turbulence: effects on the early evolution of cumulus cloud droplet spectra. *J. Atmos. Sci.* **55**, 1965–1976.

SHILLER, L. & NAUMANN, A. 1933 Über die grundlegenden berechungen bei der schwerhraftaufbereitung. *Ver. Deut. Ing.* **77**, 318.

SQUIRES, K. D. & EATON, J. K. 1991 Preferential concentration of particles by turbulence. *Phys. Fluids* A **3**, 1169–1179.

SUNDARAM, S. & COLLINS, L. R. 1996 Numerical considerations in simulating a turbulent suspension of finite-volume particles. *J. Comput. Phys.* **124**, 337–350.

SUNDARAM, S. & COLLINS, L. R. 1997 Collision statistics in an isotropic, particle-laden turbulent suspension. *J. Fluid Mech.* **335**, 75–109.

WANG, L.-P. & MAXEY, M. R. 1993 Settling velocity and concentration distribution of heavy particles in homogeneous isotropic turbulence. *J. Fluid Mech.* **256**, 27–68.

WANG, L.-P. & STOCK, D. E. 1992 Stochastic trajectory models for turbulent diffusion: Monte-Carlo process versus Markov chains. *Atmos. Environ.* **26**, 1599–1607.

WANG, L.-P. & STOCK, D. E. 1993 Dispersion of heavy particles by turbulent motion. *J. Atmos. Sci.* **50**, 1897–1913.

WANG, L.-P., WEXLER, A. S. & ZHOU, Y. 1998*a* On the collision rate of small particles in isotropic turbulence. Part 1. Zero-inertia case. *Phys. Fluids* **10**, 266–276.

WANG, L.-P., WEXLER, A. S. & ZHOU, Y. 1998*b* Statistical mechanical descriptions of turbulent coagulation. *Phys. Fluids* **10**, 2647–2651.

WANG, L.-P., WEXLER, A. S. & ZHOU, Y. 2000 Statistical mechanical description and modeling of turbulent collision of inertial particles. *J. Fluid Mech.* **415**, 117–153.

WILLIAMS, J. J. E. & CRANE, R. I. 1979 Drop coagulation in cross-over pipe flows of wet steam. *J. Mech. Engng Sci.* **21**, 357–360.

WILLIAMS, J. J. E. & CRANE, R. I. 1983 Particle collision rate in turbulent flow. *Intl J. Multiphase Flow* **9**, 421–435.

YUU, S. 1984 Collision rate of small particles in a homogeneous and isotropic turbulence. *AIChE J.* **30**, 802–807.

XIONG, Y. & PRATSINIS, S. 1991 Gas phase production of particles in reactive turbulent flows. *J. Aerosol Sci.* **22**, 637–655.

ZHOU, Y., WEXLER, A. S. & WANG, L.-P. 1998 On the collision rate of small particles in isotropic turbulence. Part 2: Finite inertia case. *Phys. Fluids* **10**, 1206–1216.